

The role of spinal concave–convex biases in the progression of idiopathic scoliosis

Mark Driscoll · Carl-Eric Aubin · Alain Moreau ·
Isabelle Villemure · Stefan Parent

Received: 19 August 2008 / Revised: 1 October 2008 / Accepted: 14 December 2008 / Published online: 8 January 2009
© Springer-Verlag 2008

Abstract Inadequate understanding of risk factors involved in the progression of idiopathic scoliosis restrains initial treatment to observation until the deformity shows signs of significant aggravation. The purpose of this analysis is to explore whether the concave–convex biases associated with scoliosis (local degeneration of the intervertebral discs, nucleus migration, and local increase in trabecular bone-mineral density of vertebral bodies) may be identified as progressive risk factors. Finite element models of a 26° right thoracic scoliotic spine were constructed based on experimental and clinical observations

that included growth dynamics governed by mechanical stimulus. Stress distribution over the vertebral growth plates, progression of Cobb angles, and vertebral wedging were explored in models with and without the biases of concave–convex properties. The inclusion of the bias of concave–convex properties within the model both augmented the asymmetrical loading of the vertebral growth plates by up to 37% and further amplified the progression of Cobb angles and vertebral wedging by as much as 5.9° and 0.8°, respectively. Concave–convex biases are factors that influence the progression of scoliotic curves. Quantifying these parameters in a patient with scoliosis may further provide a better clinical assessment of the risk of progression.

M. Driscoll · C.-E. Aubin · I. Villemure
Ecole Polytechnique de Montréal,
Biomedical Engineering Institute, P.O. Box 6079,
Station Centre Ville, Montreal, QC H3C 3A7, Canada

M. Driscoll · C.-E. Aubin · A. Moreau · I. Villemure · S. Parent
Research Center Sainte-Justine University Hospital,
3175 Cote Sainte-Catherine Road, Montreal,
QC H3T 1C5, Canada

A. Moreau
Department of Stomatology, Faculty of Dentistry,
Université de Montréal, PO Box 6128, Station Centre Ville,
Montreal, QC H3C 3J7, Canada

A. Moreau
Department of Biochemistry, Faculty of Medicine,
Université de Montréal, PO Box 6128, Station Centre Ville,
Montreal, QC H3C 3J7, Canada

C.-E. Aubin (✉)
Ecole Polytechnique de Montreal, Mechanical Engineering
Department, Canada Research Chair
CAD Innovations in Orthopedic Engineering,
NSERC/Medtronic Industrial Research Chair in Spine
Biomechanics, P.O. Box 6079, Station Centre Ville,
Montreal, QC H3C 3A7, Canada
e-mail: carl-eric.aubin@polymtl.ca

Keywords Scoliosis · Growth modulation ·
Hemiepiphysiodesis · Finite element model

Introduction

Scoliosis is a musculoskeletal deformity defined by a lateral and rotational curvature of the spine. This affects 3–4% of the population of which 80% are idiopathic. There are several theories that attempt to describe its etiology, however no individual or exclusive cause has yet to emerge from this ongoing investigation. Notwithstanding, it is generally accepted that an important factor in the progression of such deformity is founded on the Hueter–Volkman principle [19]. This principle distinguishes how non physiological loading of epiphyseal plates will modify regular growth patterns. When extended to the pathomechanism of scoliosis, it essentially defines how asymmetric loading of the vertebral bodies leads to the progression of the deformity. This phenomenon is further

supported by the frequent clinical observation of local vertebral deformations in the form of wedging within scoliotic spines [3, 26, 39]. The dynamics responsible for such alteration has been verified by several authors and has been quantified through the process of *in vivo* experimentation on various species [34]. The resulting growth/force relationships have then been integrated into finite element models in order to forecast progression of selected spinal configurations [33, 38]. The predictive ability of these simulations highlights the importance of maintaining physiological loading conditions within the spine during pubertal growth.

Although spinal loads are induced by muscular activity, body weight, and subject dynamics, the morphology and mechanical properties of tissues surrounding the vertebral growth plates nonetheless manipulate local stress distribution. More specifically, the health of the intervertebral disc, the migration of the nucleus pulposus, and the trabecular bone mineral density (BMD) have each been identified as factors involved in local stress elevations [11, 14, 18]. Adams et al. have shown that a degenerated disc becomes the main source of load transfer against the adjacent endplate (formerly the growth plate in immature vertebra) [1]. Also, they have demonstrated that damaged trabecular arcades lead to high stress concentrations in the apposing annulus [2]. Keller et al., among others, have shown a close correlation between intervertebral disc degeneration and underlying trabecular BMD [15]. Degenerated discs and increased trabecular BMD undergo an increase in mechanical modulus [9, 21]. These mechanical biases may then generate local increase in the stress levels of the surrounding growth plate. Such concept of stress shielding, due to altered mechanical properties, has been recognized to play a role in the etiology of posttraumatic osteoarthritis of knee articular cartilage [13]. This is propagated by a local increase in BMD, which allows for a greater load support and thus the associated increased rate of cartilage wear. Within the spinal column, the described concave–convex biases are known to cause elevated risk levels of failure in endplates [25] but their role in the progression of idiopathic scoliosis has never been explored.

The geometric configuration of a scoliotic spine entails remodeling of both the discs and the trabecular bone due to unbalanced loading between the concave and convex sides of the curve. Elevated levels of BMD have been quantified to occur in the concave side of the curvature when compared against measurements taken from the convex side [31]. The annulus of adolescent scoliotic spines have been reported to show signs of degeneration on the concave portions [10, 37]. Also, an offset of the geometric centre of mass in vertebral bodies, due to altered BMD, was correlated to the degree of nucleus migration in adolescents with idiopathic scoliosis [28, 29].

The objective of this article is to test the hypothesis that the lateral concave–convex biases of scoliotic spines play a role in the progression of the deformity by altering stress distribution over the growth plates.

Materials and methods

The geometry of two finite element models (FEM) was constructed on the bases of patient specific characteristics obtained from a stereo-radiographic reconstruction technique, which provided 3D coordinates of 17 points per vertebra [4]. The patient under consideration had a right thoracic curve of 26° Cobb (apex at T7) with a normal sagittal profile. The resulting FEM consisted of approximately 35,000 elements governed by linear elastic behaviour (Fig. 1). The models were composed of seventeen anterior vertebral bodies from T1 to L5 and 16 intervertebral discs, while including nine anatomical partitions with material properties that reflect findings from published studies (Table 1). These partitions include: the cortical shell; two trabecular portions dividing lateral concave and convex sections; two divisions for the annulus fibrosus, also with a concave–convex division; nucleus pulposus; and the vertebral growth plates constructed in three sections, as previously explored [36]. In this study, the zones of the vertebral growth plates were constructed in three sections, namely a sensitive zone, a newly formed bone layer, and a transition zone. The sensitive zone includes the physiological reserve, proliferative and upper hypertrophic regions of the growth plate. The newly formed bone area includes the lower hypertrophic region in which bone calcification occurs. The rate at which local bone growth occurs in this section is governed by the stress levels experienced in the above sensitive layer [30]. The transition region links the above sensitive and newly formed bone regions to the underlying trabecular bone and its cortical shell (Fig. 1). The applied spinal forces are based on load distribution, as reported by Schultz [32], and defined by a body weight (BW) distribution of 14% on T1 with an addition of 2.6% on the following vertebral bodies, ending at L5 with 57% of BW. A “follower load” of a magnitude of 20% BW, with force vectors tangential to curvature profile, was also added to BW to emulate the forces and stability provided by the surrounding muscles [27]. The boundary conditions of the model were provided by a restraint on the inferior extremity of L5 in all degrees of freedom during loading and growth simulations.

The nucleus within the disc remained laterally centered in the model without biases, while its position was governed by a correlation derived from MRI analyses that determined the nucleus position in patients with idiopathic scoliosis in the model including the discussed concave–convex biases [29].

Fig. 1 **a** Posterior view of FEM; **b** vertebral body with growth plate divisions; **c** stress zones of interest on vertebral growth plate

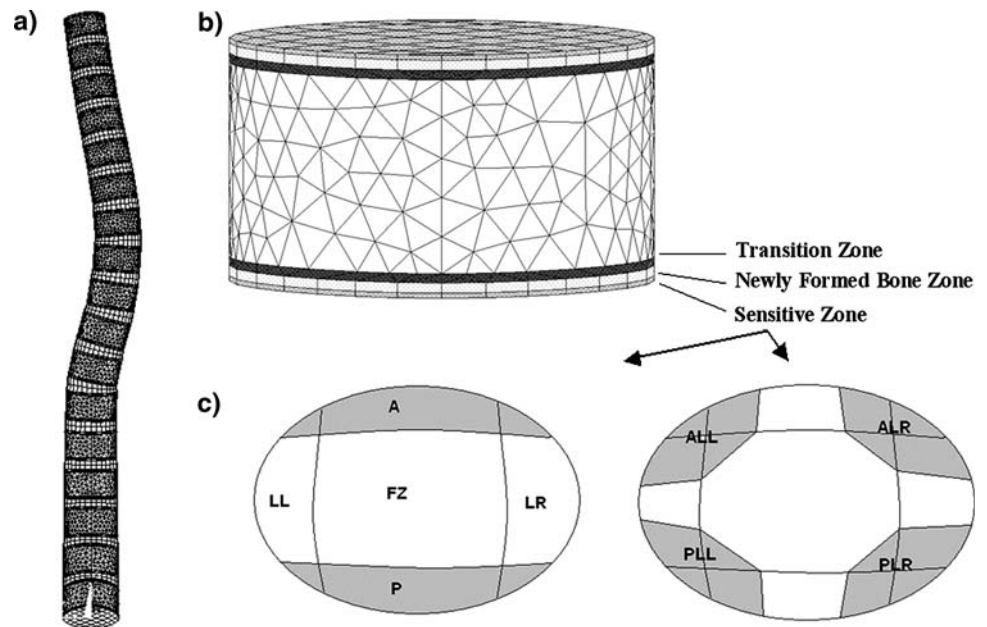


Table 1 Material properties of different anatomical structures of the FEM

Tissue	Zone	Model w/out biases		Model w/ biases		
		Young's modulus (MPa)	Poisson's ratio	Young's modulus (MPa)		Poisson's ratio
				Concave	Convex	
Growth Plate	Sensitive	12	0.4	12	12	0.4
	Newly formed bone	100	0.3	100	100	0.3
	Transition	300	0.3	300	300	0.3
Intervertebral disc	Nucleus	2	0.49	2	2	0.49
	Annulus	8	0.45	8 to 10	8	0.45
Vertebral body	Cortical bone	14,500	0.3	14,500	14,500	0.3
	Cancellous bone	400	0.3	400 to 429.6	400	0.3

Its displacement from the lateral geometric center was defined as a function of its wedge angle. However, the mechanical properties of the nucleus were homogenous throughout the spine in both models. The Young's modulus of both the annulus and the trabecular regions were uniform in the model without biases whereas different concave–convex moduli were programmed to be representative of their location within the curvature of the spine in the model with biases. The elastic modulus distribution within the discs respect experimental results from complementing studies [17, 42]. The local concave stiffness of the annulus was attributed a modulus associated with discs of grade 2 degeneration (Nachemson score) whereas the modulus of the convex portion was considered that of a healthy disc. The modulus of the concave section of the trabecular bone was acquired by following correlations describing the offset of the geometric center of mass [28], while the convex portion was maintained at 400 MPa. Equilibrium relations were then used, while assuming a lateral 50–50 division, to achieve the

ratio of BMD between the concave and convex regions. These ratios were then converted into BMD magnitudes respecting statistical CT measurements taken from vertebral bodies of stage II tanner subjects [6]. Finally, a local modulus bias was achieved by converting the difference in BMD to a bias in mechanical properties within the trabecular region using correlations obtained from pig vertebrae [24].

The analysis of the modulus bias impact was performed in two parts. The first part was achieved by executing a detailed stress analysis of the sensitive layer of the vertebral growth plates of the models with and without the concave–convex biases (trabecular bone and annulus moduli with nucleus migration). Results were then compared and the differences in growth plate stress distribution were quantified. This interpretation consisted of acquiring the longitudinal stress, perpendicular to the growth plate, on the 7,000 nodes of the sensitive layers in each spine model. Because it is the sensitive layer that responds to stress and regulates the level of growth in the vertebra [30],

it was divided into nine zones of interest: flex zone (FZ), lateral left (LL), lateral right (LR), anterior (A), posterior (P), anterior lateral left (ALL), anterior lateral right (ALR), posterior lateral left (PLL), and posterior lateral right (PLR) (Fig. 1). The mean stress across each zone of the growth plates was determined by taking the average longitudinal stress acting on all nodes within the division. This simulation was then repeated while individually including the nucleus migration, annulus stiffness bias, and trabecular bone stiffness bias, in order to interpret the influence each factor has on altering stress distribution over the growth plates.

The second part of the analysis performed iterative computations in order to simulate the growth of an adolescent spine for both models (Fig. 2). A progression of one year was simulated at 3-month intervals where each iteration consisted of four sub-steps. First, loading was applied followed by evaluation of the stress levels (σ) registered in the growth plates' sensitive zone. The scaled (β) difference, between these stress levels (σ) and those measured under regular conditions (σ_m), were converted into a thermal loading and applied on the adjoined elements in the newly formed bone layer. The thermal expansion (G) of the elements in this layer simulated the respective mechanical growth modulation as a ratio of the otherwise uniform growth (G_m).

$$G = G_m(1 - \beta(\sigma - \sigma_m)) \quad [34]$$

$$\beta = 1.7 \text{ MPa}^{-1}$$

$$\sigma_m = 0.1 - 0.02 \text{ MPa}$$

$$G_m = 0.8 - 1.1 \text{ mm year}^{-1} \quad [5]$$

Stress analysis, which included assessment of sagittal and coronal Cobb angles as well as vertebral wedging, was performed after each growth iteration.

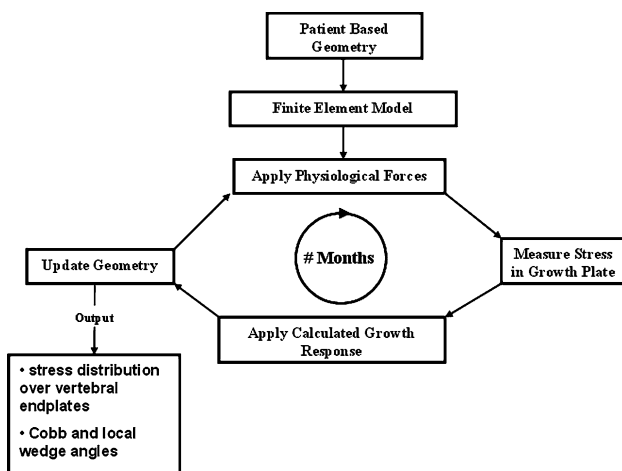


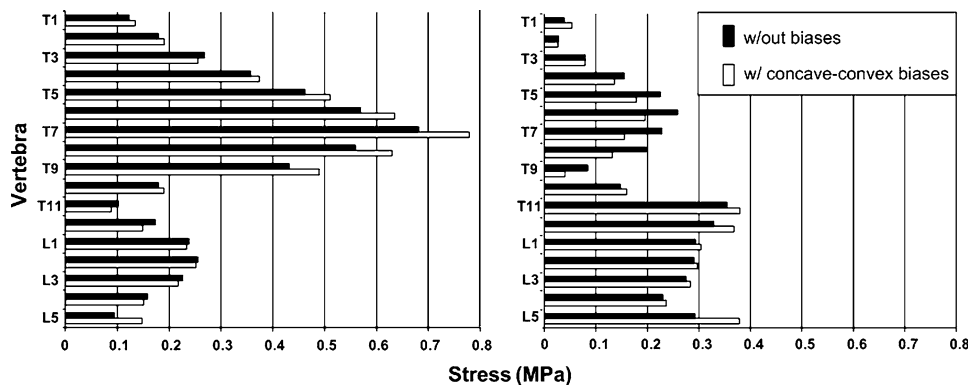
Fig. 2 Block diagram of algorithm pattern controlling growth simulation

Prior to the analysis, the model was validated through several steps. The stress profile, measured within the intervertebral disc of the L4–L5 functional unit, was compared to the magnitude and distribution of those measured in vivo by Wilke in various positions [40]. Also, load sharing between the cortical and trabecular regions in the vertebral body, was compared with ratios acquired via compression testing of excised thoracic vertebra [16]. In addition, a sensitivity analysis was performed in order to explore the relative contribution to the loading assumption compared to the explored concave–convex biases. This was achieved by simulating different loading applications (gravitational load, follower load, and a scaled combination of both gravitational and follower loads) and quantifying the change in stress distribution relative to those imposed by the explored concave–convex biases. Finally, in order to isolate the influence of the concave–convex biases from spinal configuration, the calculated concave–convex inequalities (Table 1) for the right-thoracic model were integrated into a third FEM. This model was attributed a normal alignment, thus perfectly aligned in the coronal plane with a sagittal profile matching the other models, and the described growth simulation was performed.

Results

The concave–convex biases for the spine model with a right thoracic Cobb of 26° were determined to be a 2 MPa increase of the modulus in the concave portion of the annulus, up to 29.6 MPa increase in the concave section of the trabecular bone when compared to convex portion, and a nucleus migration of up to 2 mm towards the convexity of the spine. Stress distribution in the right thoracic model without these biases showed the presence of asymmetrical loading on the growth plates. Figure 3 shows how the coronal curvature creates non-uniform stress distribution between the lateral left (concave) and right (convex) subdivisions. The greatest difference occurred in the apex T7 at 0.46 MPa, with the lateral left section measuring 0.68 MPa and the lateral right showing 0.22 MPa. Results from running identical simulations, in the model that included the effect of a migrating nucleus and mechanical concave–convex biases in the trabecular and annulus, are also displayed in Fig. 3. The analysis returned very similar stress profiles for the anterior and posterior zones of interest in the growth plates. However, it returned a stress increase on the concavity of the curve (LL) and a stress reduction on the convexity (LR) of the thoracic region, while the opposite effect was observed in the lumbar region. This difference is most prominent at the apex of the curvature T7 at 0.63 MPa, with lateral left and right stresses of 0.78 and 0.15 MPa respectively. Therefore the

Fig. 3 **a** Lateral left and **b** lateral right stress distribution across vertebral growth plates of spine model with and without concave–convex factors



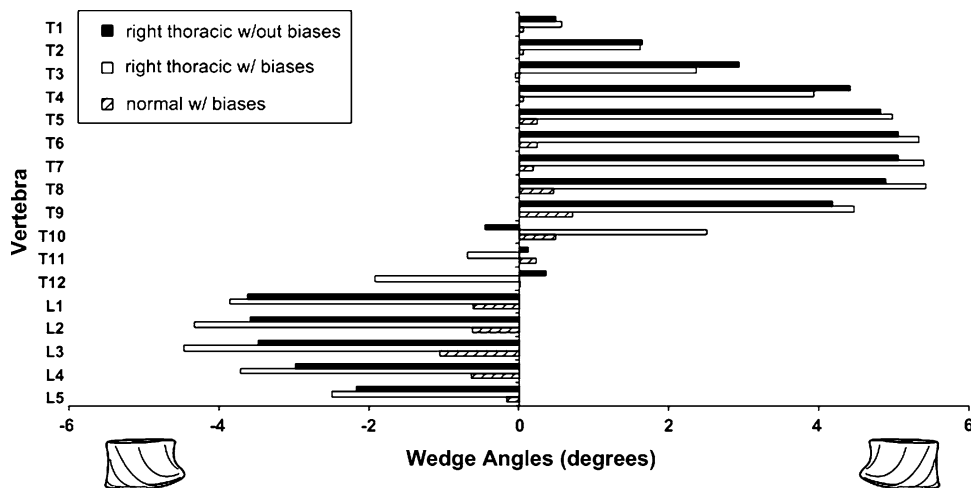
relative difference at the apex imposed by including the biases was found to be 0.17 MPa or a 37% increase over regular stress distribution without the presence of the biases. This increase in asymmetric stress caused by the concave–convex biases varied in the thoracic curve between 18% at T4 and 29% at T9 whereas stress manipulation was less prominent in the lumbar region. The individual contribution of the concave–convex biases, to the increase in asymmetrical loading of T7, was calculated to be 43% due to annulus stiffness bias, 22% from the trabecular stiffness bias, and 35% evolved from nucleus migration.

Results from growth simulations performed under the above conditions further highlighted the influence of concave–convex biases. There was negligible progression of lordosis and kyphosis defined by insignificant vertebral wedging in the sagittal reference plane. However, the Cobb angles and vertebral wedging in the coronal plane progressed over the length of the simulations. Figure 4 displays the vertebral wedging in the coronal plane after one year of progression for the models with and without the integration of the concave–convex biases. The wedge angles for both cases share the same pattern with a slight discrepancy at T11–T12, which becomes the inflexion

point of the new spinal configuration. The sum of vertebral wedging in the thoracic and lumbar regions are 33.0° and –15.3° respectively for the simulation performed with uniform mechanical properties, i.e. where no discrepancies between concave and convex portions were included. The same simulation performed with the presence of concave–convex biases yielded vertebral wedging sums of 36.6° at the thoracic level and –21.4° in the lumbar region.

Results from the sensitivity analysis of the concave–convex stress distribution showed prominent reliance on the loading condition as expected. However, for each loading condition the relative difference in stress distribution, as a result of including the biases, showed little variation. Finally, results from uniquely simulating the concave–convex biases in the spine model without the presence of a scoliotic curvature were obtained. Under a healthy spine configuration these biases were responsible in providing an average stress difference of 0.04 MPa between what was previously convex and concave sections. When a growth simulation was performed on this model, results included a vertebral wedge sum of 2.7° and –3.1° in the thoracic and lumbar regions respectively along with a vertebral wedge pattern that followed results observed in the model with a right thoracic curve (Fig. 4).

Fig. 4 Magnitudes of coronal vertebral wedge angles after 1 year scoliotic progression with and without biases as well as for a normal spinal configuration with biases



Discussion

The mechanical influence of increased vertebral BMD, annular degeneration, and nucleus migration in scoliotic spines was explored. These biases were included in a finite element model and modified stress distribution over the growth plate as well as played a moderate role in the progression of scoliotic deformities. For a spine model with an initial right thoracic Cobb angle of 26°, inclusion of these biases increased the difference in concave–convex growth plate stress distribution by up to 37% (0.17 MPa) at the apical vertebra. The recorded differences in lateral stress distribution agreed with *in vivo* measurements taken from the discs of patients with scoliosis [20]. Although this reported study obtained hydrostatic pressure measurements from patients positioned laterally with loading conditions unlikely simulated in this study, this close agreement demonstrates the qualitative corroboration of the model in terms of stress prediction. This increase in asymmetrical stresses, caused by the inclusion of the concave–convex biases, provoked an additional progression of 3.6° in the thoracic region and 5.9° in the lumbar portion when compared with simulations without the integration of the curvature biases.

These results support the hypothesis that the explored biases alter the force transmission path within the spine. The remodeled and more rigid concave portion assumes dominance over the load distribution and thus increases asymmetrical stresses within the vertebral growth plates. This, in a sense, provides stress shielding of the convexity of the vertebral growth plates in scoliotic spines. The notion of this load stress shielding in the spinal column is further supported by the close correlation found between local annulus degeneration and elevated levels of trabecular BMD in the underlying vertebral body [23]. Grant et al. [8] also demonstrated this phenomenon by quantifying increased endplate strength in areas of degenerated discs and elevated trabecular BMD. Such correlations demonstrate that these factors complement each other by increasing the weight bearing capacity due to internal remodeling. The bone remodeling process, once initiated, becomes a dynamic cycle governed by Wolf's Law [41], where the concave portion becomes stiffer, while the convex portion weakens. This model does not include algorithms that control the level of internal remodeling as a function of stress stimulus. The present model interprets the level of degeneration of the disc and the remodeling of the trabecular bone to be constant, as a function of initial configuration. As mentioned, these parameters were obtained by following *in vivo* correlations derived from adolescents with idiopathic scoliosis. These internal biases would increase with time, and thus the inclusion of these adjustments would augment the magnitude of their impact on the progression of the deformity.

The elevated stiffness of the concave annulus accounted for 43% of the increase in asymmetrical loading of the vertebral growth plates as compared to 22% for bone remodeling and 35% for nucleus migration, suggesting that annulus remodeling primarily contributes to the increase of growth plate compressive stresses and consequent growth modulation on the spine. The significance of this factor respects previous predictions by Nachemson [22] and is supported by the works of Adams et al. [1], who described that a degenerated disc would entail a transfer of compressive stresses from the nucleus to the degenerated annulus. In a scoliotic spine, it is likely that nucleus migration occurs foremost, while degenerative remodeling of the annulus precedes trabecular apposition. Hence, the prominent stress altering role of the annulus (observed in this analysis) would have greater impact in the later stages of scoliosis progression. However, the onset and early stages of scoliosis would evolve without the presence or influence of the explored biases as they develop as a result of the condition in its advanced stages rather than suggest causative factors. Therefore the investigated biases are not speculated to have a role in the etiology of scoliosis, alternatively their progressive influence on the pathomechanism was hypothesized and demonstrated.

The loading of the spine has been integrated into the model without any prejudice from its configuration. Other authors have explored the impact of muscle activation strategies [35] or muscle weakening [12] in the progression of the deformity. However, in this analysis, loading was not altered during iterations. Results from the sensitivity analysis provided evidence of the importance of loading conditions on the stress distribution. However, simulations with and without the presence concave–convex biases were performed on identical models in order to isolate and explore the role of these biases while excluding the influence of loading techniques on the results. Therefore this study explores the relative difference imposed by the concave–convex biases and upon examination this difference proved robust under a variety of loading conditions. When the spine model with a healthy configuration, was submitted to the mild bias in properties associated with a right thoracic Cobb angle of 26°, progression of the deformity prevailed and followed the patterns that would have otherwise occurred in the scoliotic spine. These findings further support the unconditional impact that the presence of concave–convex biases has on stress distribution over the vertebral growth plate and, in conjunction, longitudinal vertebral growth rates in scoliotic progression.

The model was limited to the anterior portion of the spine as this study aimed to explore the variation in axial stress distribution over the growth plate. Moreover, roughly 90% of axial compressive loads are believed to be transmitted within the anterior section of the spine [7] thus

supporting the models as suitable and relevant platforms for the explored analyses. The correlations used in this analysis represent the mean values of concave–convex biases as a function of spinal configuration. Patient specific values of these parameters, although difficult to obtain, would yield a more personalized investigation of the progressive influence of these biases. However, the developed model may be used to identify spinal configurations in which the differences in concave–convex properties become significant progressive risk factors.

Conclusion

This novel analysis provides evidence that the presence of concave–convex biases is a secondary risk factor that influences the progression of established and advanced scoliotic curves by augmenting the magnitude of asymmetrical stresses in the vertebral growth plates. Quantifying these parameters in a patient with scoliosis may improve progression forecasting.

Acknowledgments Funded by the Natural Sciences and Engineering Research Council of Canada, Medtronic Sofamor Danek and the Canada Research Chair Program.

References

- Adams M, McNally D, Dolan P (1996) Stress distribution inside intervertebral discs. The effects of age and degeneration. *J Bone Joint Surg* 78:965–972. doi:10.1302/0301-620X78B6.1287
- Adams M, McNally D, Wagstaff J, Goodship A (1993) Abnormal stress concentrations in lumbar intervertebral discs following damage to the vertebral bodies: a cause for disc failure? *Eur Spine J* 1:214–221. doi:10.1007/BF00298362
- Aubin CE, Dansereau J, Petit Y, Parent S, De Guise J, Labelle H (1998) Three-dimensional measurement of wedged scoliotic vertebrae and intervertebral discs. *Eur Spine J* 7:59–65. doi:10.1007/s005860050029
- Delorme S, Petit Y, De Guise J, Aubin CE, Dansereau J (2003) Assessment of the 3-D reconstruction and high-resolution geometrical modeling of the human skeletal trunk from 2-D radiographic Images. *IEEE Trans Biomed Eng* 50:989–998. doi:10.1109/TBME.2003.814525
- Dimeglio A, Ferran J (1990) Three-dimensional analysis of the hip during growth. *Acta Orthop Belg* 56:111–114
- Gilsanz V, Boechat M, Roe T, Loro M, Sayre J, Goodman W (1994) Gender difference in vertebral body sizes in children and adolescents. *Radiology* 190:673–677
- Goel K, Clausen J (1998) Prediction of load sharing among spinal components of a C5–C6 motion segment using the finite element approach. *Spine* 23(6):684–691. doi:10.1097/00007632-199803150-00008
- Grant J, Oxland T, Dvorak M, Fisher C (2002) The effects of bone mineral density and disc degeneration on the structural property distribution in the lower lumbar vertebral endplates. *J Orthop Res* 20:1115–1120. doi:10.1016/S0736-0266(02)00039-6
- Guerin H, Elliott D (2006) Degeneration affects the fiber reorientation of human annulus fibrosus under tensile load. *J Biomech* 39:1410–1418. doi:10.1016/j.jbiomech.2005.04.007
- He Y, Qiu Y, Zhu Z (2006) Quantitative analysis of types I and II collagen in the disc annulus in adolescent idiopathic scoliosis. *Stud Health Technol Inform* 123:123–128
- Horst M, Brinckmann P (1981) Measurement of the distribution of axial stress on the end-plate of the vertebral body. *Spine* 6(3):217–232. doi:10.1097/00007632-198105000-00004
- Huynh A, Aubin CE, Mathieu P, Labelle H (2007) Simulation of progressive spinal deformities in duchenne muscular dystrophy using a biomechanical model integrating muscle and vertebral growth modulation. *Clin Biomech (Bristol, Avon)* 22:392–399. doi:10.1016/j.clinbiomech.2006.11.010
- Kamibayashi L, Wyss U, Cooke T, Zee B (1995) Trabecular microstructure in the medial condyle of the proximal tibia of patients with knee osteoarthritis. *Bone* 17(1):27–35. doi:10.1016/8756-3282(95)00137-3
- Keller T, Hansson T, Abram A, Spengler D, Panjabi M (1989) Regional variations in the compressive properties of lumbar vertebral trabeculae. Effects of disc degeneration. *Spine* 14(9):1012–1019. doi:10.1097/00007632-198909000-00016
- Keller T, Ziv I, Moeljanto E, Spengler D (1993) Interdependence of lumbar disc and subdiscal bone properties: a report of the normal and degenerated spine. *J Spinal Disord* 6(2):106–113. doi:10.1097/00002517-199304000-00003
- Kilincer C, Inceoglu S, Sohn M, Ferrada L, Bakirci N, Benzel E (2007) Load sharing within a human thoracic vertebral body: an in vitro biomechanical study. *Turk Neurosurg* 17:167–177
- Li S, Patwardhan A, Amirouche F, Harvey R, Meade K (1995) Limitations of the standard linear solid model of intervertebral disc subject to prolonged loading and low-frequency vibration in axial compression. *J Biomech* 28:779–790. doi:10.1016/0021-9290(94)00140-Y
- McNally D, Adams M (1992) Internal intervertebral disc mechanics as revealed by stress profilometry. *Spine* 17(1):66–73. doi:10.1097/00007632-199201000-00011
- Mehlman C, Arachi A, Roy D (1997) Hyphenated history: the Hueter–Volkman law. *Am J Orthop* 26:798–800
- Meir A, Fairbank J, Jones D, McNally D, Urban J (2007) High pressures and asymmetrical stresses in the scoliotic disc in the absence of muscle loading. *Scoliosis* 2:4. doi:10.1186/1748-7161-2-4
- Mitton D, Rumelhart C, Hans D, Meunier P (1997) The effects of density and test conditions on measured compression and shear strength of cancellous bone from the lumbar vertebrae of ewes. *Med Eng Phys* 19:464–474. doi:10.1016/S1350-4533(97)00001-5
- Nachemson A (1965) In vivo discometry in lumbar discs with irregular nucleograms. Some differences in stress distribution between normal and moderately degenerated discs. *Acta Orthop Scand* 36:418–434
- Nanjo Y, Morio Y, Nagashima H, Hagino H, Teshima R (2003) Correlation between bone mineral density and intervertebral disc degeneration in pre- and postmenopausal women. *J Bone Miner Metab* 21:22–27. doi:10.1007/s007740300004
- Nielson D, McEvoy F, Madsen M, Jensen J, Svalastoga E (2007) Relationship between bone strength and dual-energy X-ray absorptiometry measurements in pigs. *J Anim Sci* 85:667–672. doi:10.2527/jas.2006-025
- Oshia R, Tencer A, Ching R (2003) Effect of loading on endplate and vertebral body strength in human lumbar vertebrae. *J Biomech* 36:1875–1881. doi:10.1016/S0021-9290(03)00211-2
- Parent S, Labelle H, Skalli W, De Guise J (2004) Vertebral wedging characteristics changes in scoliotic spines. *Spine* 29(20):E455–E462. doi:10.1097/01.brs.0000142430.65463.3a

27. Patwardhan A, Havey R (1999) A follower load increases the load-carrying capacity of the lumbar spine in compression. *Spine* 24(10):1003–1009. doi:[10.1097/00007632-199905150-00014](https://doi.org/10.1097/00007632-199905150-00014)
28. Perie D, Curnier D, De Gauzy J (2003) Correlation between nucleus zone migration within scoliotic intervertebral discs and mechanical properties distribution within scoliotic vertebrae. *Magn Reson Imaging* 21:949–953. doi:[10.1016/S0730-725X\(03\)00216-9](https://doi.org/10.1016/S0730-725X(03)00216-9)
29. Perie D, De Gauzy J, Curnier D, Hobatho M (2001) Intervertebral disc modeling using a MRI method: migration of the nucleus zone within scoliotic intervertebral discs. *Magn Reson Imaging* 19:1245–1248. doi:[10.1016/S0730-725X\(01\)00452-0](https://doi.org/10.1016/S0730-725X(01)00452-0)
30. Price J, Oyajobi B, Russell R (1994) The cell biology of bone growth. *Eur J Clin Nutr* 48:131–149
31. Rumancik S, Routh R, Pathak R, Burshell A, Nauman E (2005) Assessment of bone quality and distribution in adult lumbar scoliosis: new dual-energy X-ray absorptiometry methodology and analysis. *Spine* 30:434–439. doi:[10.1097/01.brs.0000153344.06682.b2](https://doi.org/10.1097/01.brs.0000153344.06682.b2)
32. Schultz A, Andersson G, Ortengren R, Nachemson A (1982) Loads on the lumbar spine. Validation of a biomechanical analysis by measurement of intradiscal pressures and myoelectric signals. *J Bone Joint Surg* 64:713–720
33. Stokes I (2007) Analysis and simulation of progressive adolescent scoliosis by biomechanical growth simulation. *Eur Spine J* 16:1621–1628. doi:[10.1007/s00586-007-0442-7](https://doi.org/10.1007/s00586-007-0442-7)
34. Stokes I, Aronsson D, Dimock A, Cortright V, Beck S (2006) Endochondral growth in growth plates of three species at two anatomical locations modulated by mechanical compression and tension. *J Orthop Res* 24(6):1327–1333. doi:[10.1002/jor.20189](https://doi.org/10.1002/jor.20189)
35. Stokes I, Gardner-Morse M (2004) Muscle activation strategies and symmetry of spinal loading in the lumbar spine with scoliosis. *Spine* 29:2103–2107. doi:[10.1097/01.brs.0000141182.42544.1f](https://doi.org/10.1097/01.brs.0000141182.42544.1f)
36. Sylvestre PL, Villemure I, Aubin CE (2007) Finite element modeling of the growth plate in a detailed spine model. *Med Biol Eng Comput* 45:977–988. doi:[10.1007/s11517-007-0220-z](https://doi.org/10.1007/s11517-007-0220-z)
37. Urban M, Fairbank J, Bibby S, Urban J (2001) Intervertebral disc composition in neuromuscular scoliosis: changes in cell density and glycosaminoglycan concentration at the curve apex. *Spine* 26(6):610–617. doi:[10.1097/00007632-200103150-00010](https://doi.org/10.1097/00007632-200103150-00010)
38. Villemure I, Aubin CE, Dansereau J (2002) Simulation of progressive deformities in adolescent idiopathic scoliosis using a biomechanical model integrating vertebral growth. *J Biomed Eng* 124(6):784–790
39. Villemure I, Aubin CE, Grimard G, Dansereau J, Labelle H (2001) Progression of vertebral and spinal three-dimensional deformities in adolescent idiopathic scoliosis: a longitudinal study. *Spine* 26(20):2244–2250. doi:[10.1097/00007632-200110150-00016](https://doi.org/10.1097/00007632-200110150-00016)
40. Wilke H, Neef P, Caimi M, Hoogland T, Claes L (1999) New In vivo measurements pressures intervertebral disc in daily life. *Spine* 24(8):755–762
41. Wolff J (1892) *Das Gesetz der Transformation der Knoche*. Hirshwald, Berlin
42. Yerramalli C, Chou A, Miller G, Nicoll S, Chin K, Elliot D (2007) The effect of nucleus pulposus crosslinking and glycosaminoglycan degradation on disc mechanical function. *Biomech Model Mechanobiol* 6:13–20. doi:[10.1007/s10237-006-0043-0](https://doi.org/10.1007/s10237-006-0043-0)